Journal of Molecular Catalysis A: Chemical 303 (2009) 9–14

Contents lists available at ScienceDirect

Journal of Molecular Catalysis A: Chemical

journal homepage: www.elsevier.com/locate/molcata

Review

Enhanced photocatalytic activity of bismuth molybdates with the preferentially exposed {0 1 0} surface under visible light irradiation

Yan Zheng, Fang Duan, Ju Wu, Liang Liu, Mingqing Chen, Yi Xie*

School of Chemical and Material Engineering, Jiangnan University, Lihu Road, 1800#, Wuxi 214122, PR China

ARTICLE INFO

Article history:
Received 25 July 2008
Received in revised form 16 December 2008
Accepted 16 December 2008
Available online 25 December 2008

Keywords:
γ-Bi_2MoO_6
Sheets
Exposed surface
Photocatalytic activity
Visible light irradiation

ABSTRACT

In this work, γ-Bi_2MoO_6 samples with different morphologies and surface structures were prepared via simple solution methods and their photocatalytic degradations of rhodamine-B (RhB) were investigated under visible light irradiation. In spite of their lower BET surface area, we found that the γ-Bi_2MoO_6 sheets with the preferentially exposed {0 1 0} surface exhibited the greatly enhanced photocatalytic activity. The mechanism study and structural analysis of stoichiometric γ-Bi_2MoO_6 indicated that the particular reactive surface with much more oxygen defects and in-plane vacancies, derived from the larger distortion of the MoO_6 octahedra, play a more important role of the enhanced photocatalytic activity.

Contents

1. Introduction

In recent years, the design and synthesis of catalysts with a highly reactive/selective catalysis have attracted much attention, because inexpensive transportation fuels, high-temperature lubricants, chlorine-free refrigerants, high-strength polymers, stain-resistant fibers, cancer treatment drugs, and many thousands of other products required by modern society would not be possible without the existence of catalysts [1]. And much admirable researches on the factors which may impact the catalytic properties have been investigated to progress their activity [2]. The dominating related reports have put forward that the high BET surface area is the main influencing factor of the catalysis [3]. For example, Zhao et al. have reported the preparation of the porous tin dioxide nanostructures with high surface area that exhibit excellent catalytic activity toward methanol decomposition [4]. Nevertheless, recent researches have indicated that the particular surface may also be pivotal to the catalytic activity. For instance, Li et al. have found that CeO_2 nanorods with well-defined {0 0 1} and {1 1 0} planes showed higher CO oxidation activity than CeO_2 nanoparticles because of the

* Corresponding author. Tel.: +86 510 8591 7063.
E-mail address: yxie@jiangnan.edu.cn (Y. Xie).

1381-1169/$ – see front matter © 2009 Published by Elsevier B.V.
doi:10.1016/j.molcata.2008.12.010

higher reactivity of {0 0 1} and {1 1 0} planes [5]. Another typical case may be the iron catalysts used for the synthesis of ammonia, in which the preferentially exposed {1 1 1} planes of the iron surface were observed to be crucial to generate excellent activity [6,7].

Today the improvement of photocatalytic activity is also an important challenge for its photocatalysis in splitting water into hydrogen and oxygen and degrading organic pollutants in the water or air for solving the energy shortage and the environment pollution [8–12]. Due to the potential excellent photocatalytic property under visible light, bismuth mixed oxides have attracted extensive attention these days. The Aurivillius structure of related oxides with general formula $Bi_2A_{n-1}B_nO_{3n+3}$ (A = Ca, Sr, Ba, Pb, Bi, Na, K and B = Ti, Nb, Ta, Mo, W, Fe) usually possess unique layered structures by the perovskite slabs of $(A_{n-1}B_nO_{3n+1})^{2-}$ sandwiched between $(Bi_2O_2)^{2+}$ layers which exhibit predominant photocatalytic activity [13–16]. Similarly, the previous researches have reported that the increase of the BET surface area leads to improvement of the photocatalytic activity. For example, our group has reported that the Bi_2WO_6 hierarchical nest-like structures built by higher order nanoplates alignment with large surface area which exhibited excellent photocatalytic activity [17]. Besides, some preliminary researches revealed that the photocatalytic activity may also be closely ascribed to the crystal plane of the nanosheets [18]. The monoclinic scheelite $BiVO_4$ was reported to show much higher photocatalytic activity under visible light irradiation which was mainly attributed to basal plane of (0 1 0) and the distortion of the Bi–O polyhedron [19]. As one of the three different crystallographic phases of bismuth molybdates, the γ-Bi_2MoO_6 (BMO) shows the distinguished photocatalytic activity under visible light irradiation for its suitable band gap and intrinsic structure [20–22]. Therefore, it is still very necessary to investigate the effects of the γ-Bi_2MoO_6 surface structure on their photocatalytic activity.

Herein, to demonstrate the effect of the BMO surface plane on the photocatalysis, we primarily fabricate three γ-Bi_2MoO_6 samples with different morphologies and surface structures via simple hydrothermal methods and then investigate the photocatalytic activity to rhodamine-B (RhB) under visible light irradiation. While it is well known that the suitable band gap is the precondition for its visible light responsive photocatalysis ability of photocatalysts, this work revealed that the γ-Bi_2MoO_6 sheets with the preferentially exposed {0 1 0} surface exhibited the greatly enhanced photocatalytic activity, due to the particular reactive surface with much more oxygen defects and in-plane vacancies. This result gives us inspiration that the particular reactive surface may play more important role of the enhanced photocatalytic activity except the surface area in the case of γ-Bi_2MoO_6 photocatalyst.

2. Experimental and methods

2.1. Chemicals

Sodium molybdate ($Na_2MoO_4{\cdot}2H_2O$), bismuth nitrate ($Bi(NO_3)_3{\cdot}5H_2O$), nitric acid (HNO_3) and sodium hydroxide (NaOH) were purchased from Shanghai Chemical Co. Ltd. and were used as received without further purification.

2.2. Synthesis

The following procedure was adopted for the synthesis of bismuth molybdates samples. The precursor material, Bi $(NO_3)_3{\cdot}5H_2O$ (1 mmol) was dissolved in nitric acid. Then the $Na_2MoO_4{\cdot}2H_2O$ (1 mmol) dissolved in NaOH was added into the above $Bi(NO_3)_3{\cdot}5H_2O$ solution which was stirred for about 30 min until the homogeneous solution formed and the pH value of the solution was adjusted to 9. These homogeneous solutions were then treated separately for the three samples with different morphologies and surface structures. Sample A with larger sheets was obtained while the above precursor solution were hydrothermally treated at 150 °C for 12 h in a Teflon-sealed autoclave. The obtained product were isolated by centrifugation, washed with distilled water and absolute ethanol for several times, and finally dried in a vacuum at 50 °C for 5 h. Sample B with smaller sheets was obtained in the presence of CTAB with the other conditions unchanged compared to Sample A. Sample C with irregular nanoparticles was prepared while the homogenous solution was exposed to high-intensity ultrasound irradiation (6 mm diameter Ti-horn, JK-60DT with 60W, 40 kHz) for 60 min and then was isolated by centrifugation, dried in a vacuum, and finally calcined at 500 °C for 2 h [22].

2.3. Characterization

The samples were characterized by X-ray powder diffraction (XRD) with a Japan Rigaku D/max rA X-ray diffractometer equipped with graphite monochromatized high intensity Cu Kα radiation (λ = 1.54178 Å), recorded with the 2θ ranging from 10° to 70°. The transmission electron microscopy (TEM) images were performed with a Hitachi model H-800 instrument with a tungsten filament, using an accelerating voltage of 200 kV. High-resolution transmission electron microscopy (HRTEM) images and electron diffraction (ED) patterns were carried out on a JEOL-2010 TEM at an acceleration voltage of 200 kV. The field emission scanning electron microscopy (FE-SEM) images were taken on a FEI Sirion-200 SEM. The Brunauer–Emmett–Teller (BET) surface areas were determined by nitrogen adsorption (Micromeritics ASAP 2000 system).

2.4. Photocatalytic test

Photocatalytic activities of the above samples were evaluated by the degradation of RhB under visible light irradiation of a 500 W Xe lamp. In each experiment, 0.08 g of the as-prepared BMO sample as a photocatalyst was added into 100 mL of RhB solution (10^{-5} mol/L) and the solution was stirred for one night in the dark to reach adsorption equilibrium between the catalyst and the solution. Then the solution was exposed to visible light irradiation. After irradiation for a given time, the suspensions were centrifugated to separate the samples, and the concentrations of RhB were determined every 5 min using UV–vis spectra (Shimadzu UV2550).

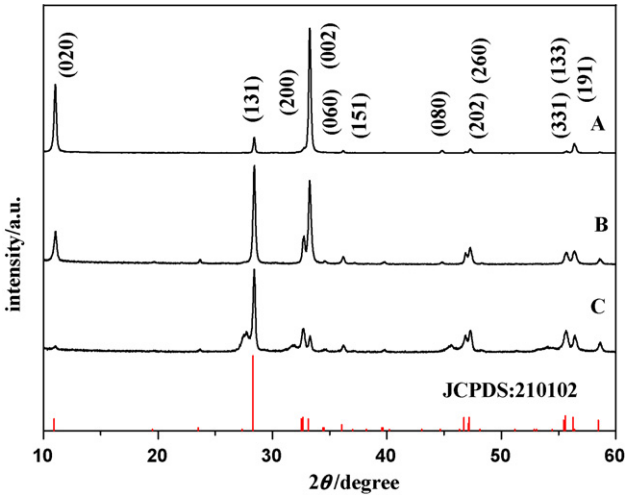

Fig. 1. The XRD pattern of the γ-Bi_2MoO_6 samples: A, larger sheets; B, smaller sheets prepared in CTAB; and C, irregular nanoparticles.

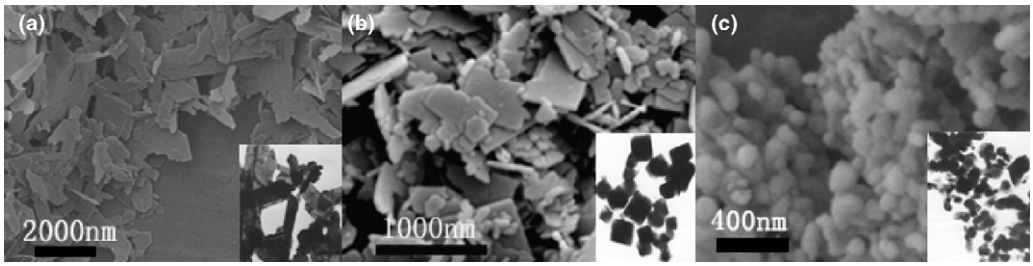

Fig. 2. The SEM and TEM images of the BMO samples: (a) larger sheets; (b) smaller sheets prepared in CTAB; and (c) irregular nanoparticles.

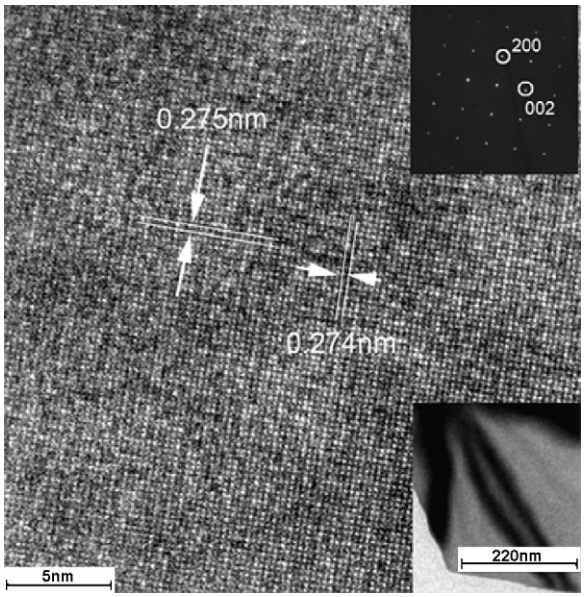

Fig. 3. The HR-TEM image on an individual γ-Bi_2MoO_6 sheet of Sample A (top inset: SAED pattern; bottom inset: TEM image).

3. Results and discussion

3.1. Structural characterization of the prepared bismuth molybdates samples

The phase and purity of the samples were determined by X-ray powder diffraction (XRD), and the typical diffraction patterns are shown in Fig. 1. All of the peaks could be readily indexed to the gamma phase of bismuth molybdate, with lattice constants of $a = 5.502$ Å, $b = 16.210$ Å, and $c = 5.483$ Å, which is found to match well with the standard XRD pattern for γ-Bi_2MoO_6 (JCPDS card No.21-0102). The morphologies of BMO samples are illuminated by FE-SEM and TEM shown in Fig. 2, in which it can be clearly seen that the Sample A and Sample B are consisted of sheets with the size of 2 and 0.8 μm, respectively, while Sample C is irregular nanoparticles with the size of 100 nm. Sheet-like characteristics of both Samples A and B could also be reflected by the XRD patterns. The significantly intensified (0 6 0) diffraction peaks compared with the characteristic (1 3 1) diffraction peak of γ-Bi_2MoO_6 reveal that there is a bias of orientations of {0 1 0} crystallographic plane. This phenomenon is also consistent with the HR-TEM observation. For example, the HR-TEM image of an individual sheet of Sample A as shown in Fig. 3 indicates their single-crystalline nature and the calculated lattice spacing of 2.75 and 2.74 Å correspond to the literature data of d (2 0 0) = 2.750 Å and d (0 0 2) = 2.741 Å, respectively. All the above characterizations give that the BMO sheets of Samples A and B with a preferred [0 1 0] orientation and the surface can be indexed as {0 1 0} surface. The selected area electron diffraction (SAED) pattern (Fig. 3 inset) reveals the clear diffraction spots with well alignment further indicate the single-crystal nature of the sheets. The bias of orientation of {0 1 0} surface also explains the intensified (0 6 0) peaks in the XRD pattern. Due to the surface-structure-dependent reactivity, the highly oriented surfaces could be of great meaning for both theoretical investigations and technological application.

3.2. UV–vis DRS and BET analysis of the prepared bismuth molybdates samples

To estimate the band gaps of the photocatalysts, the UV–vis diffuse reflectance spectra (DRS) of the above BMO samples were measured by using a UV–vis spectrometer, as shown in Fig. 4a. The all three samples offer the photoabsorption property from the UV light region to visible light shorter than 480 nm. The steep shape of the spectra indicates that the visible light absorption is not due to the transition from the impurity level but is due to the band-gap transition [23]. Following the equation $ah\nu = A(h\nu - E_g)^{n/2}$ [16], the band gaps of the above samples were estimated from the onset of the absorption edge (in Fig. 4b). These results point out that all these samples have a band gap suitable for photocatalytic degradation

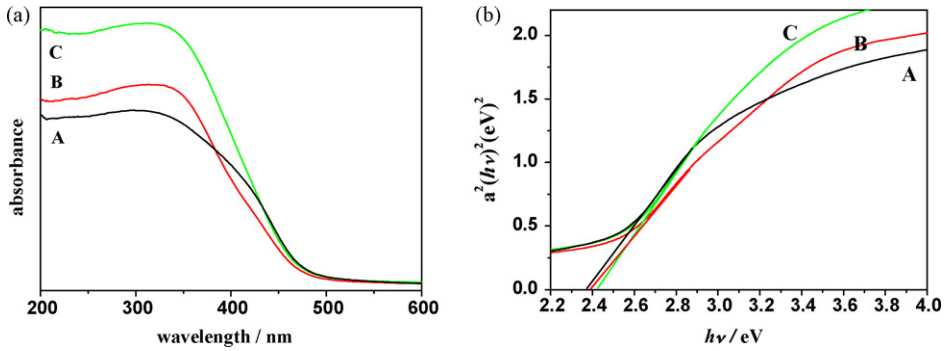

Fig. 4. (a) UV–vis diffuse reflectance spectra of the γ-Bi_2MoO_6 samples and (b) plots of $a^2(h\nu)^2(eV)^2$ vs. photon energy ($h\nu$): A, larger sheets; B, smaller sheets prepared in CTAB; and C, irregular nanoparticles.

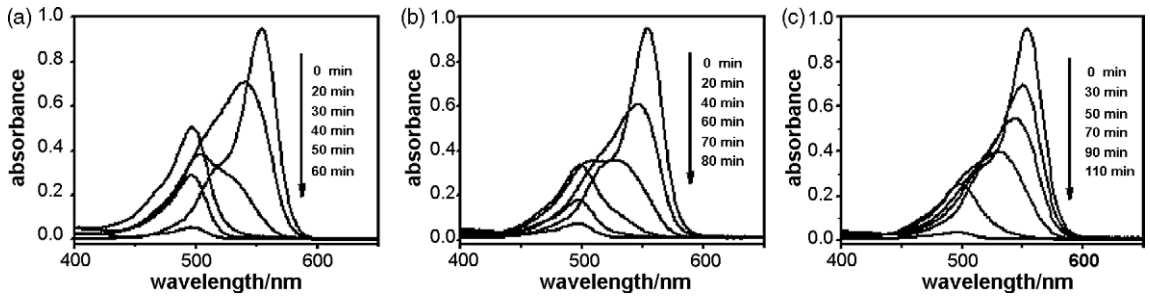

Fig. 5. UV–vis spectral changes of RhB (10^{-5} mol/L) as a function of irradiation time in the presence of the BMO as catalyst: (a) larger sheets; (b), smaller sheets prepared in CTAB; and (c) irregular nanoparticles.

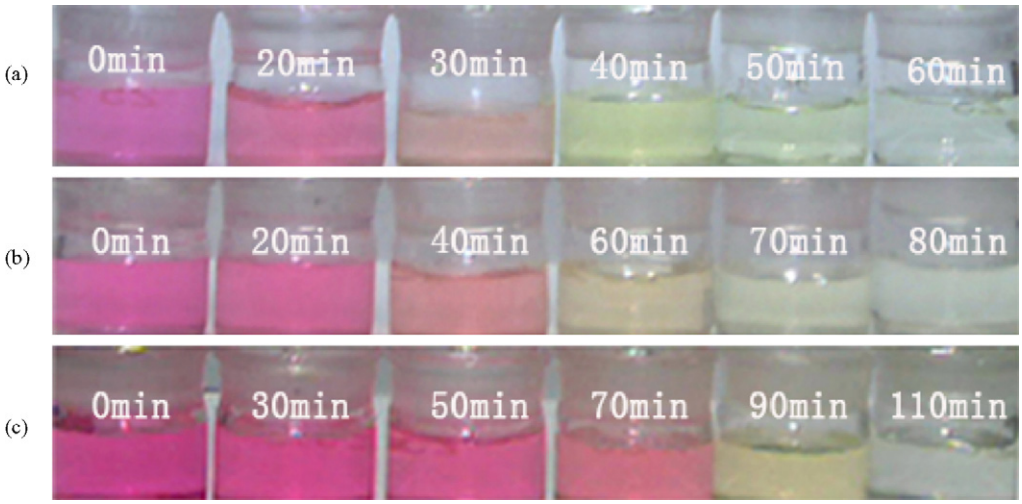

Fig. 6. The photos of the RhB solution color changed with the presence of the prepared samples through the increasing time: (a) larger sheets; (b) smaller sheets prepared in CTAB; and (c) irregular nanoparticles.

of organic pollutants under visible light irradiation. The band gap of the Sample A is little smaller than that of the Samples B and C, in consistent with that the band gap energy of semiconductor nanoparticles increase with the decrease of grain size and are not largely affected by the preparation and morphology of the samples. Moreover, the BET surface areas of above samples reveal that Sample A consisted of larger sheets exhibits the smallest surface area in the three samples, whereas Sample C with the irregular nanoparticles possesses the largest surface area due to their smallest size.

3.3. Photocatalytic activity of the prepared γ-Bi_2MoO_6 samples

The photocatalysis tests indicate that Sample A of the larger sheets with lowest surface area perform the most excellent photocatalytic property on degradation of the RhB solution under visible light irradiation. During the process of RhB dye decomposition in water solution under visible light irradiation, the intense pink color of the starting RhB solution with the presence of Sample A with larger sheets almost faded completely only with the exposure time increasing to 60 min (shown in Figs. 5 and 6) much shorter than other samples with the larger surface areas. Also, the enhanced photocatalysis ability of the Samples A and B are recorded in Fig. 7 which show the degradation efficiency of the RhB by the spots of C/C_0 vs. irradiation time, here C was the concentration of the rest fully *N*,*N*,*N*′,*N*′-tetraethylated rhodamine with a major absorption band at λ_{max} = 552 nm which were obtained by peak curve-fitting [24], when C_0 was the initial concentration of the RhB solution. From Fig. 7, it is also clearly seen that the photodegradation efficiency of RhB over Sample A was nearly 99% after 30 min irradiation. The green-yellow color of Sample A solution at 30 min shown in Fig. 6 was caused by the intermediated product of rhodamine decomposition, in consistent with the peak curve-fitting results.

3.4. Photocatalysts mechanism study

It is well known that photocatalysts with higher surface areas can adsorb RhB molecules more efficiently and tend to perform admirable photocatalytic activity under visible light irradiation. However, in our work the larger sheet-like Sample A with the preferentially exposed {0 1 0} surface but lowest BET value exhibited

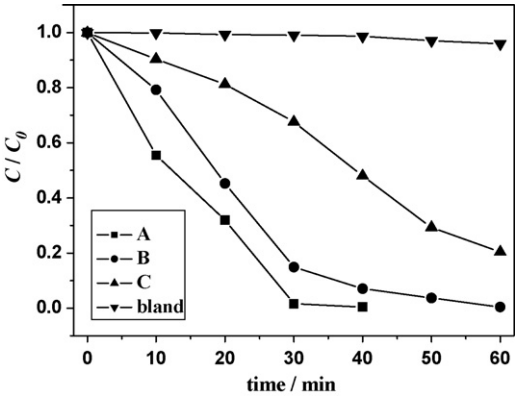

Fig. 7. The photocatalytic degradation of the fully *N*,*N*,*N*′,*N*′-tetraethylated rhodamine under the visible light irradiation in the presence of the prepared BMO samples: A, larger sheets; B, smaller sheets prepared in CTAB; and C, irregular nanoparticles.

more excellent photocatalytic activity than other samples with higher BET surface areas. Then, a question was raised: what factors influence the photocatalysis except the surface areas? Based on the mechanism study on the photocatalysis of bismuth tungstate and titanium dioxide [16,25], the photocatalytic degradation of organic compounds with the presence of γ-Bi_2MoO_6 was proposed. At first, the γ-Bi_2MoO_6 photocatalysts can absorb visible light to generate electron/hole pairs (reaction (1)) because of their suitable band gap. The holes (BMO (h_{vb}^+)) are subsequently hunted by the ubiquitously present molecular H_2O to yield •OH radicals (reaction (2)). Concurrently, the electrons (BMO (e_{cb}^-)) at the BMO surface are scavenged by the adsorbed molecular oxygen to yield the superoxide radical anion $O_2^{\bullet -}$ first (reaction (3)), hence on protonation yields the •OOH radicals (reaction (4)). Degradation of RhB solution can subsequently occur through either •OH and/or •OOH radical attack on the conjugated structure of RhB (reaction (5)). On the other hand, from the UV–vis spectral changes of RhB solution in the presence of BMO photocatalyst shown in Fig. 5, it is clearly shown that the absorption blue-shifted from 552 to 498 nm with the increasing time, which was indicated that the RhB molecules were de-ethylated in a stepwise manner. Because RhB molecules can absorb the visible light in range 460–600 nm, namely the RhB molecular can be excited by visible light and converted to be RhB* (reaction (6)). The electrons transfer from the excited chemisorbed RhB_{ads}^* molecules to the BMO surface, which are immediately injected into the conduction band of BMO to generated BMO (e_{cb}^-) (reaction (7)) and react with the surface absorbed O_2 molecules to yield the •OOH (as reactions (3) and (4)), during that process the RhB_{ads}^* are converted to radical $RhB_{ads}^{\bullet +}$ which should be de-ethylated step by step (reaction (9)). At the same time, some chemisorbed RhB molecules on the BMO surface can be directly converted to be radical $RhB_{ads}^{\bullet +}$ by the holes (BMO (h_{vb}^+)) (reaction (8)) and further degraded by the •OH and/or •OOH radicals (reaction (9)). Then all the de-ethylated intermediates were further degraded by the •OH and/or •OOH radicals (reaction (10)). Here, competitive reactions between de-ethylation and cleavage of the conjugated structure take place on the surface of the BMO samples.

$$EMO + h\nu \rightarrow BMO(e_{cb}^-) + BMO(h_{vb}^+) \quad (1)$$

$$BMO(h_{vb}^+) + OH^-(H_2O) \rightarrow {}^\bullet OH + H^+ + BMO \quad (2)$$

$$BMO(e_{cb}^-) + O_2 \rightarrow O_2^{\bullet -} + BMO \quad (3)$$

$$O_2^{\bullet -} + H^+ \rightarrow {}^\bullet OOH \quad (4)$$

$$^\bullet OOH/^\bullet OH + RhB \rightarrow \text{destruction of the conjugated structure} \quad (5)$$

$$RhB + h\nu \rightarrow RhB* \quad (6)$$

$$RhB_{ads}* + BMO \rightarrow RhB_{ads}^{\bullet +} + BMO(e_{cb}^-) \quad (7)$$

$$BMO(h_{vb}^+) + RhB \rightarrow RhB_{ads}^{\bullet +} + BMO \quad (8)$$

$$^\bullet OOH/^\bullet OH + RhB_{ads}^{\bullet +} \rightarrow \text{de-ethylated intermediates} \quad (9)$$

$$^\bullet OOH/^\bullet OH + \text{de-ethylated intermediates} \rightarrow \text{destruction of the conjugated structure} \quad (10)$$

$$BMO(e_{cb}^-) + V_o^{\bullet\bullet} \rightarrow V_o^\bullet + BMO \quad (11)$$

$$V_o^\bullet + O_2 \rightarrow O_2^{\bullet -} + V_o^{\bullet\bullet} \quad (12)$$

From the above reaction, we can confer that the photocatalysis can be enhanced with reducing the surface recombination of electrons (BMO (e_{cb}^-)) and holes (BMO (h_{vb}^+)) and increasing the concentration of •OH and/or •OOH radicals. Analysis on the structure of stoichiometric γ-Bi_2MoO_6 may give us more hints, and the structure of the stoichiometric bismuth molybdates (0 1 0) surface and the schematic crystal structures of γ-Bi_2MoO_6 were shown in Fig. 8, where we indicate the terminology used for different kinds of surface atoms and the striking feature of the surface. On the preferentially exposed {0 1 0} surface of γ-Bi_2MoO_6 sheets, MoO_6 octahedra with relatively larger distortion supply lots of oxygen defects ($V_o^{\bullet\bullet}$) formed from the unstable bridge oxygen and in-plane vacancies from the intrinsic structure of the surface which are both in favor of enhancing the photocatalytic activity. Accordingly, the presence of much more $V_o^{\bullet\bullet}$ defects on the surface of the sample no doubtedly benefit the efficient separation of electron–hole pairs to reduce the energy lost for the electron–hole recombination. Since the $V_o^{\bullet\bullet}$ defects on the γ-Bi_2MoO_6 surface play a role as the electron acceptors and convert to be $V_o^\bullet$ momentarily (reaction (11)) to restrain the recombination of electrons (BMO (e_{cb}^-)) and holes (BMO (h_{vb}^+)) on the surface and then the $V_o^\bullet$ are easily hunted by the adsorbed molecular oxygen to further produce the superoxide radical anion $O_2^{\bullet -}$ (reaction (12)) whence on protonation generate the •OOH radicals. Thus, on the sheets surface, in the competition with the de-ethylation, the cleavage of the conjugated structure by •OH/•OOH radicals is the dominant reaction. It is ascribed to the exposed {0 1 0} surface with much more oxygen defects which is prone to restrain the recombination of electron–hole pairs but impel to generate •OOH radicals. Moreover, the in-plane vacancies of the exposed {0 1 0} surface can easily trap more molecular H_2O and O_2 which lead to further increase in the concentration of •OH and/or •OOH radicals and thus maximize the photocatalytic efficiency. In this case, the cleavage on the conjugated structure become dominant process; at the same time de-ethylation of RhB molecules become a subordinate process. The latter is generally regarded as a chemisorbed controlled process, which will be accelerated by the larger BET surface area.

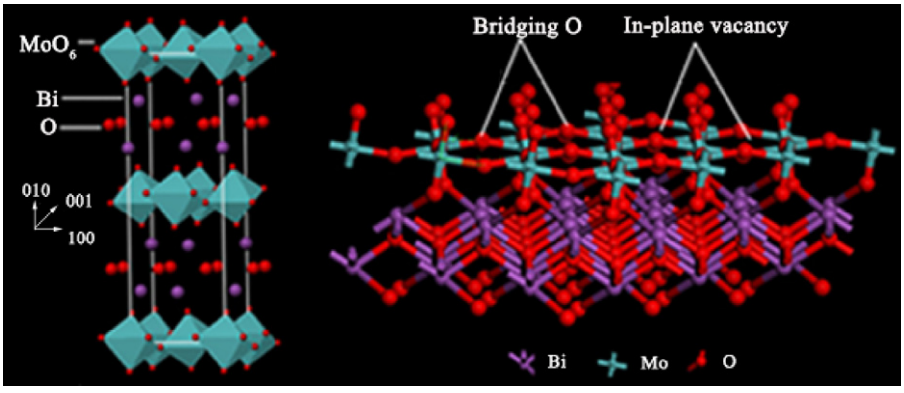

Fig. 8. (Left) The schematic crystal structures of γ-Bi_2MoO_6 composed of MoO_6 octahedral layers and Bi–O layers and (right) the (0 1 0) surface of γ-Bi_2MoO_6, showing the terminology used for difference types of surface atoms.

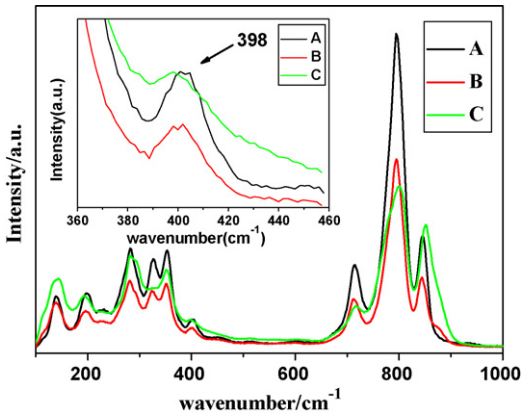

Fig. 9. The Raman spectrum of γ-Bi_2MoO_6: A, larger sheets; B, smaller sheets prepared in CTAB; and C, irregular nanoparticles.

Sample B consisted of smaller sheets prepared in the presence of CTAB show superior photocatalysis than the Sample C, but less excellent than Sample A with the larger sheets, which can be reasonably explained by the adsorption of CTAB surfactants on the BMO surface. The adsorption of the possible rudimental CTAB no doubtly decreased the exposed reactive surface areas and further restrains the generation of the •OH and/or •OOH radicals, which in reverse give evidences on the effect of the preferentially exposed {0 1 0} surface of γ-Bi_2MoO_6.

Raman spectroscopy has been proven to be a powerful tool in the characterization of the structures of transition-metal oxides as bulk phases and two-dimensional surface phases. It is well known that different molecular structures are expected to have different types of bonds which can be recorded as "fingerprint" frequencies by Raman spectroscopy. For bismuth molybdate compounds, a direct relationship has been formulated between its metal–oxygen Raman stretching frequencies and bond lengths [26]. Specially, the Raman spectral features for distorted MoO_6 octahedron in γ-Bi_2MoO_6 can be characterized by the Mo–O stretching frequencies at 398 cm^{-1}. The Raman spectrum of the as-prepared γ-Bi_2MoO_6 samples shown in Fig. 9 reveal that the sheets samples of Samples A and B have much stronger and sharper peaks at 398 cm^{-1} than the particles (Sample C) indicating the more distorted MoO_6 octahedra in the exposed surface of the sheets samples. So, Raman spectra also give the accessional but strong evidence that the large distortion of MoO_6 octahedra in the exposed {0 1 0} surface play a core role in the enhanced photocatalyst activity.

4. Conclusions

In summary, γ-Bi_2MoO_6 samples with different morphologies and surface structures were prepared via simple hydrothermal methods and their photocatalytic degradation of rhodamine-B was investigated under visible light irradiation. Since it is the known that the suitable band gap as the precondition takes the responsibility for its visible light responsive photocatalytic ability of γ-Bi_2MoO_6, we believe that except the larger surface area, the exposed reactive surface may contribute much more to the enhanced photocatalytic activity. In this work, the larger sheets sample with the preferentially exposed {0 1 0} surface of the largely distorted Mo–O octahedra supply more oxygen defects and in-plane vacancies, which enhances the concentration of •OH and/or •OOH radicals and thus improves the photocatalytic property. Hence, the photocatalytic property has a close relationship with the structure of the exposed surface plane, in that the particular reactive surface with much more oxygen defects and in-plane vacancies can greatly enhance the photocatalytic activity.

Acknowledgment

This work was supported by the National Natural Science Foundation of China (20671043).

References

[1] A.T. Bell, Science 299 (2007) 1688.
[2] H.X. Li, Z.F. Bian, J. Zhu, Y.F. Lu, J. Am. Chem. Soc. 129 (2007) 4538.
[3] Y. Zhou, M. Antonietti, J. Am. Chem. Soc. 125 (2003) 14960.
[4] Q.R. Zhao, Z.G. Zhang, Y. Xie, J. Phys. Chem. B 110 (2006) 15152.
[5] K.B. Zhou, X. Wang, X.M. Sun, Y.D. Li, J. Catal. 229 (2005) 206.
[6] G.A. Somorjai, Proceedings of the Robert A. Welch Foundation Conferences on Chemical Research, Heterogeneous Catalysis, vol. XXV, Houston, TX, November 9–11, 1981, p. 83.
[7] G. Ertl, Proceedings of the Robert A. Welch Foundation Conferenceson Chemical Research, Heterogeneous Catalysis, vol. XXV, Houston, TX, November 9–11, 1981, p. 179.
[8] A. Kudo, K. Omori, H. Kato, J. Am. Chem. Soc. 121 (1999) 11459.
[9] K. Maeda, K. Teramura, D.L. Lu, K. Domen, Nature 440 (2006) 295.
[10] Satoshihorikoshi, Aikosaitou, Ndhisaohidaka, Environ. Sci. Technol. 37 (2003) 5813.
[11] H.X. Li, Z.F. Bian, J. Zhu, Y.F. Lu, J. Am. Chem. Soc. 129 (2007) 8406.
[12] H.X. Li, X.Y. Zhang, Y.N. Huo, J. Zhu, Environ. Sci. Technol. 41 (2007) 4410.
[13] L.S. Zhang, W.Z. Wang, Z.G. Chen, L. Zhou, J. Mater. Chem. 17 (2007) 2526.
[14] C. Zhang, Y.F. Zhu, Chem. Mater. 17 (2005) 3537.
[15] Y. Zheng, J. Wu, F. Duan, Y. Xie, Chem. Lett. 36 (2007) 520.
[16] H.B. Fu, C.S. Pan, W.Q. Yao, Y.F. Zhu, J. Phys. Chem. B 109 (2005) 22432.
[17] J. Wu, F. Duan, Y. Zheng, Y. Xie, J. Phys. Chem. C 111 (2007) 12866.
[18] H.L. Xu, W.Z. Wang, W. Zhu, J. Phys. Chem. B 110 (2006) 13829.
[19] L. Zhang, D.R. Chen, X.L. Jiao, J. Phys. Chem. B 110 (2006) 2668.
[20] G.W. Keulks, L.D. Krenzke, T.M. Notermann, Adv. Catal. 27 (1978) 183.
[21] Y. Shimodaira, H. Kato, H. Kobayashi, A. Kudo, J. Phys. Chem. B 110 (2006) 17790.
[22] L. Zhou, W.Z. Wang, L.S. Zhang, J. Mol. Catal. A: Chem. 268 (2007) 195.
[23] A. Kudo, I. Tsuji, H. Kato, Chem. Commun. 17 (2002 1958).
[24] (a) T. Watanabe, T. Takizawa, K. Honda, J. Phys. Chem. 81 (1977 1845); (b) T. Inoue, T. Watanabe, A. Fujishima, K. Honda, K. Kohayakawa, J. Electrochem. Soc. 124 (1977) 719.
[25] T.X. Wu, G.M. Liu, J.C. Zhao, J. Phys. Chem. B 102 (1998) 5845.
[26] D.H. Franklin, E.W. Israel, J. Phys. Chem. 95 (1991) 10763.